Magnetic properties of self-assembled Co nanorods grown on Cu(110)-(2×3)N

Xiao Dong Ma,[1,2] Takeshi Nakagawa,[1,3] Yasumasa Takagi,[1,3] Marek Przybylski,[2] Fred M. Leibsle,[4] and Toshihiko Yokoyama[1,3,*]

[1]*Department of Structural Molecular Science, The Graduate University for Advanced Studies (Sokendai), Myodaiji-cho, Okazaki, Aichi 444-8585, Japan*

[2]*Max-Planck-Institut für Mikrostrukturphysik, Weinberg 2, 06120 Halle, Germany*

[3]*Department of Molecular Structure, Institute for Molecular Science, Myodaiji-cho, Okazaki, Aichi 444-8585, Japan*

[4]*Department of Physics, University of Missouri at Kansas City, 5110 Rockhill Road, Kansas City, Missouri 64110, USA*

(Received 28 June 2008; revised manuscript received 25 August 2008; published 24 September 2008)

Structural and magnetic properties of self-assembled Co nanorods on a Cu(110)-(2×3)N surface have been investigated by low-energy electron diffraction (LEED), Auger-electron spectroscopy (AES), magneto-optical Kerr effect (MOKE), and x-ray magnetic circular dichroism (XMCD). The LEED observation confirms that the Co nanorod grows epitaxially along the $[1\bar{1}0]$ axis and its interval exhibits the (1×6) periodicity. The AES clarifies that the N atom locates always at the surface even after 5 monolayer (ML) Co deposition. Angle dependent magnetization curves of the Co nanorods recorded by MOKE and XMCD show that the magnetic easy axis is perpendicular to the rod within the substrate plane, irrespective of the Co thickness down to 0.8 ML. This implies that the magnetic anisotropy is not dominated by the shape anisotropy but by the magnetocrystalline anisotropy. The XMCD sum-rule analysis reveals significant enhancement of the orbital magnetic moment along the easy axis compared to the hard axes. The magnetocrystalline anisotropy is found to be directly related to the anisotropy of the orbital magnetic moment.

DOI: 10.1103/PhysRevB.78.104420 PACS number(s): 75.30.Gw, 75.70.Ak, 75.75.+a, 78.20.Ls

I. INTRODUCTION

Magnetism of low-dimensional materials is one of the most attractive current issues because of technological requirements for higher density recording media as well as a fundamental interest in particle size effects on the magnetic properties. Several pioneering works concerning magnetism of nanodots, nanopillars, and nanorods on the surfaces of well-defined single-crystal substrates have been published so far.[1–9] Gambardella *et al.*[1] reported one-dimensional ferromagnetism of Co atomic chains grown on a Pt(997) stepped surface. They also observed peculiar magnetic anisotropy of the atomic chains that shows perpendicular magnetization with respect to the chain axis.[2] Elmers and co-workers[3,4,6] investigated Fe one-layer ribbons on stepped W(110), which shows the two-dimensional property from the critical behavior close to the Curie temperature.

Recently, York and Leibsle[10] discovered self-assembled growth of well-extended Co nanorods on Cu(110)-(2×3)N by the scanning tunnel microscopy (STM) measurements. The Co nanorods are extended along the $[1\bar{1}0]$ direction with six times intervals along the [001] direction. It is interesting that the second layer Co begins to grow before the nanorods coalesce with each other. The growth fashion of Co on Cu(110)-(2×3)N is essentially different from that on clean Cu(110), where Co forms randomly distributed islands.[11–14] It is also known that squarely arranged Co nanodots are formed on Cu(001)-c(2×2)N,[9] interestingly suggesting that N-terminated surfaces play a crucial role for the nanostructure formation.

In the present study, we have investigated structural and magnetic properties of the Co nanorods grown on the Cu(110)-(2×3)N substrate by *in situ* characterization techniques as low-energy electron diffraction (LEED), Auger-electron spectroscopy (AES), magneto-optical Kerr effect (MOKE), and x-ray magnetic circular dichroism (XMCD). The AES measurement gives important information on the location of the N atoms after Co deposition. The phenomenological magnetic anisotropy constants obtained by the angle-dependent magnetization curve measurements are comparatively discussed with the anisotropy of the orbital magnetic moments determined by the XMCD analysis.

II. EXPERIMENTS

A Cu(110) single crystal was mechanically polished using alumina ultrafine powder with mirror finish and subsequently cleaned in an ultrahigh vacuum (UHV) chamber[15] with the base pressure of $\sim 1\times 10^{-10}$ Torr by repeated cycles of Ar^+ sputtering and annealing at ~900 K. N was deposited by the N^+ bombardment (ion energy of 500 eV, ion current of ~1 μA) for 5–10 min and subsequent annealing at ~473 K to yield the (2×3)N surface.[10] Although the annealing temperature of ~473 K is lower than the previous report,[10] the temperature is found to be sufficiently high to yield the clear (2×3) LEED pattern. Co was deposited on the surface at ambient temperature using a commercial beam evaporator. The Co thickness d_{Co} was calibrated with respect to the Co/Cu(001) film, implying that the Co density of $2/a_0^2$ corresponds to 1 monolayer (ML), where a_0 is the lattice constant of bulk fcc Cu.

Magnetization curves were recorded by *in situ* MOKE with the longitudinal/polar configurations using a laser diode (cw, 635 nm, 5 mW) with the incidence angle of 45° and a conventional UHV-compatible electromagnet (maximum of 0.3 T). The two longitudinal MOKE geometries (magnetic field always parallel to the reflection plane) were taken with the rod axis, $[1\bar{1}0]$, parallel and perpendicular to the reflec-

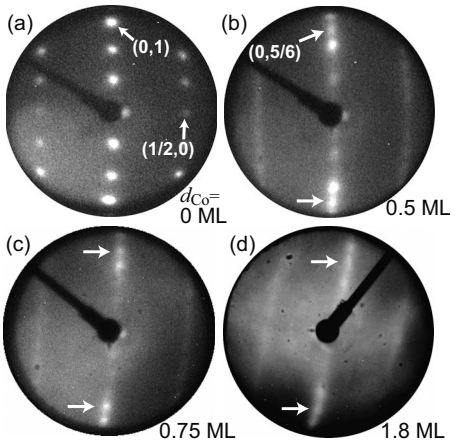

FIG. 1. LEED patterns of Co/Cu(110)-(2×3)N with (a) d_{Co} =0.0 ML, (b) 0.50 ML, (c) 0.75 ML, and (d) 1.80 ML, obtained with the primary electron energies of 29 eV at [(a)–(c)] 298 K and (d) 90 K.

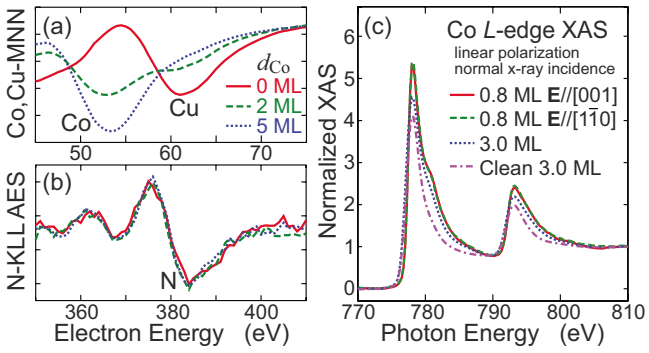

FIG. 2. (Color online) (a) N-KLL and (b) Co- and Cu-MNN AES of Co/Cu(110)-(2×3)N with d_{Co}=0.0, 2.0, and 5.0 ML. (c) Linearly polarized normal-incidence Co *L*-edge XAS of Co/Cu(110)-(2×3)N with d_{Co}=0.8 ML (red solid, green dashed) and 3.0 ML (blue dotted), and 3 ML Co on clean Cu(110) (pink dashed-dotted). In the spectra of d_{Co}=0.8 ML, azimuthal angle dependence with the electric-field vector **E** parallel (∥[1$\bar{1}$0], green dashed) or perpendicular (∥[001], red solid) to the rod axis is also shown.

tion plane. This allows one to investigate the magnetic anisotropy along [1$\bar{1}$0] and [001]. Temperature-dependent longitudinal MOKE along the [001] axis was also examined.

The *in situ* Co *L*-edge x-ray absorption spectra (XAS) and XMCD measurements were performed using total electron yield mode at the bending magnet station beamline 4B at UVSOR-II in Institute for Molecular Science.[15,16] We conducted two kinds of *in situ* XMCD experiments. The first run dealt with d_{Co} dependence at T=90 K and $H=\pm 0.15$ T using an electromagnet by switching the magnetic field or the x-ray helicity (circular polarization factor of $P_c=\pm 0.70$). In the second run, the magnetic anisotropy was investigated using a recently installed UHV-compatible superconducting magnet (7 T) with a liquid He cryostat (sample temperature of 4.9 K) and a sample preparation chamber. The Co/Cu(110)-(2×3)N sample was prepared in the preparation chamber and was transferred to the superconducting magnet chamber under the UHV condition. Since the background pressure of the magnet chamber is always in the 10^{-11} Torr range owing to the presence of liquid He reservoir, the sample pollution during the sample transfer and the XMCD measurements can be avoided. Details of the XMCD measurement system are given in the literature.[17]

III. RESULTS AND DISCUSSION

A. Structural properties

Figure 1 shows the LEED patterns of Co/Cu(110)-(2×3)N. Superposing the inherent (2×3) periodicity shown in Fig. 1(a), the (1×6) superstructure spots are clearly visible after Co deposition up to 1.8 ML [see arrows in Figs. 1(b)–1(d)]. The measurement temperature of 1.8 ML Co [Fig. 1(d)] is 90 K, while the other images were taken at 298 K. The superstructure spots of 1.8 ML Co are more streaky at 298 K than at 90 K. The (1×6) periodicity is consistent with the previous STM observation,[10] and thus the present LEED observations confirm the growth of Co nanorods. Moreover, we have performed systematic STM observations for many kinds of metal atoms on Cu(110)-(2×3)N including the present system and have confirmed the formation of the nanorods. The STM work will be published elsewhere.[18]

Figures 2(a) and 2(b) show, respectively, N-KLL and Co- and Cu-MNN AES to verify the thickness dependence of Co. The N-KLL AES intensity is constant even after the deposition of d_{Co}=5 ML, while the Cu-MNN AES is significantly attenuated after the deposition of d_{Co}=2 ML and almost completely disappears at d_{Co}=5 ML. These findings imply that the N atom is located near the top of the surface as long as the Co coverage is more than 2 ML. The Cu atom, on the other hand, does not significantly diffuse onto the surface. Such a behavior is similar to the case of Co/Cu(001)-*c*(2×2)N.[19] Since the Co deposition on clean Cu(110) leads to the formation of randomly distributed Co islands,[10,14] the N atom can be regarded as a surfactant that effectively modifies the growth fashion of deposited films. Besides aiding in the formation of nanorods as a surfactant, these top N atoms may also play a crucial role in protecting the underneath Co nanorods from the contaminations of ambient residual gas in the UHV chamber. This is important for the present *in situ* XMCD work because the magnetic anisotropy of the Co film on clean Cu(110) is known to show great time dependence due to CO adsorption.[14] Owing to this effect, the nanorods investigated here hold very stable and long-life magnetization.

Figure 2(c) depicts the Co *L*-edge XAS of d_{Co}=0.8 and 3.0 ML on Cu(110)-(2×3)N, together with that of 3.0 ML Co on clean Cu(110). The spectra were taken at normal incidence of linearly polarized x rays. In the 0.8 ML spectra, the azimuthal angle dependence, where the x-ray electric-field vector **E** is parallel to the [001] or [1$\bar{1}$0] axis, is also shown, although the two spectra are essentially identical. The detailed analysis procedure will be described in Sec. III C. Huge differences in the white line intensity are seen among those of the three different samples. The $L_{3,2}$ white line intensity is noticeably enhanced on the (2×3)N-covered sur-

face compared to that on the clean one, and the spectra of d_{Co}=0.8 ML show more intense white line features than the one of d_{Co}=3.0 ML. Moreover, the shoulder structure at a higher energy side (~782 eV) emerges more clearly. Since the white line intensity reflects the 3*d* hole number and the shoulder structure may be attributable to the multiplet splitting of cationic Co, these findings suggest that the Co atoms in Co/Cu(110)-(2×3)N are considerably ionized. It should be noted that the spectrum of 3 ML Co on Cu(110)-(2×3)N still shows a stronger white line and the shoulder structure than that of the clean one. By combining the above AES result, one can conclude that the surface Co atom forms direct chemical bonds with N.

The growth fashion of the Co nanorods on Cu(110)-(2×3)N should be discussed here. The N deposition induces the drastic reconstruction of the Cu(110) surface from inherent twofold symmetry to nearly fourfold symmetry;[20] the local structure around N closely resembles that of Cu(001)-c(2×2)N. On the contrary, the Co deposition on Cu(110)-(2×3)N leads to the nanorod formation that exhibits again the twofold symmetry. This may originate from the significant corrugation of the surface layer along the [001] direction. Although the Cu(110)-(2×3)N surface looks nearly fourfold symmetry in an atomic scale, the magnitude of the corrugation is as much as ~0.5 Å and the surface maintains the twofold symmetry in a larger (nanometer) scale.

The present finding that the N atom locates always at the top surface can be explained qualitatively in a simple thermodynamic consideration. The surface energy of Co (392.7 kJ/mol) is larger than that of Cu (313.4 kJ/mol). This indicates possible Cu migration on the top surface when Co is deposited on clean Cu(110). In Cu(110)-(2×3)N, however, the surface is stabilized in the presence of adsorbate N. The N atom forms rather covalent (though partially ionic as described above) bonds with metals and the coordination number of metal atoms around N should be smaller than that of the metal-metal bonds. This implies that the N atom is likely to locate at the surface. This is true for most typical elements such as S and C, which are often embedded in the bulk metals as impurities and come up to the surface when the metals are annealed. When Co is deposited on Cu(110)-(2×3)N, the N atom migrates to the surface by breaking the N-Cu bonds and creating the N-Co ones. This is at least thermodynamically reasonable; the Co-N bond should be stronger than the N-Cu one since the Co 3*d* electrons can participate in the N-Co bonding more effectively than the Cu 3*d* electrons in the N-Cu bonding. For more quantitative discussion including dynamical processes, sophisticated quantum-mechanical calculations will be required.

B. MOKE in d_{Co}>1.5 ML

The magnetic properties of Co/Cu(110)-(2×3)N with d_{Co}>1.5 ML, where the Co nanorods coalesce to some extent, were at first investigated. The anisotropy of the magnetization curves (Kerr rotation angles) of d_{Co}=2.0 ML is depicted in Fig. 3(a). The curve along the [001] axis shows the rectangular-shaped hysteresis, while no prominent magnetization is seen either along [1$\bar{1}$0] or [110]. This clearly implies that the magnetic easy axis is [001] at this coverage, which is perpendicular to the rod axis within the substrate plane. The easy axis of [001] is in accordance with the Co islands grown on clean Cu(110).[11,12] The magnetization curves of Co on clean Cu(110) are shown for 5 ML Co in the inset of Fig. 3(b), which confirm the easy axis of [001]. Since the N atoms diffuse to the surface in the present sample, the interface interaction between Co and Cu might be similar between the (2×3)N and clean surfaces, yielding the same easy axis that is dominated by the magnetocrystalline anisotropy.

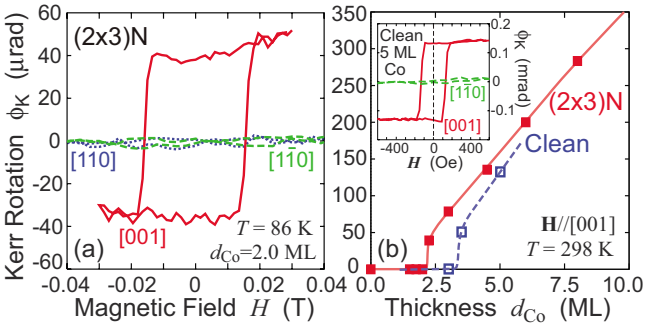

FIG. 3. (Color online) (a) Magnetization curves of Co/Cu(110)-(2×3)N (d_{Co}=2.0 ML) at T=86 K taken by the two longitudinal (**M**∥[001] and **M**∥[1$\bar{1}$0]) and one polar (**M**∥[110]) MOKE configurations. The nanorod axis is [1$\bar{1}$0]. (b) Thickness dependence of the magnetization of Co on the Cu(110)-(2×3)N and clean Cu(110) surfaces at T=298 K. The inset in (b) shows the magnetization curves of Co on clean Cu(110) at T=298 K taken by the longitudinal MOKE along the axes of [001] and [1$\bar{1}$0].

The difference of the magnetic properties between N-terminated and clean surfaces can be found in the critical thickness d_c at room temperature, as shown in Fig. 3(b). The critical thickness, where the spontaneous magnetization appears at room temperature, is estimated as ~2.2 ML for Co/Cu(110)-(2×3)N, which is noticeably smaller than ~3.3 ML for Co/clean Cu(110). It is well known that on clean Cu(110) Co exhibits an island growth mode.[10,13,14] Although Co growth on the Co/Cu(110)-(2×3)N surface does not show a layer-by-layer growth fashion either, the coalescent nanorods may form a larger magnetic unit than the island, resulting in higher critical temperature and smaller critical thickness, which are close to those of the layer-by-layer grown Co on Cu(001).[21]

We also measured temperature dependence of magnetization in order to obtain critical temperature. Figure 4(a) shows the magnetization curves (Kerr rotation angles) of d_{Co}=1.5 ML. In contrast to the rectangular shape in the hysteresis curve of d_{Co}=2.0 ML in Fig. 3(a), the hysteresis curve of d_{Co}=1.5 ML is rather smooth, indicating the presence of more isolated nanorods in this coverage. Figure 4(b) depicts corresponding temperature dependence of the saturated Kerr rotation angles for d_{Co}=1.5, 2.0, and 3.0 ML. The critical temperatures T_c were obtained as ~78.5 K (d_{Co}=1.5 ML), ~220 K (2.0 ML) and >300 K (3.0 ML). Note also that the Kerr rotation angle is considerably attenuated in d_{Co}=2.0 and 1.5 ML compared to d_{Co}=3.0 ML. The Kerr rotation angle of

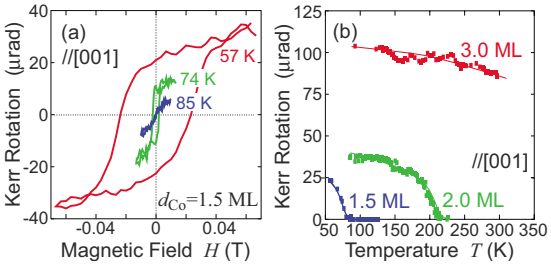

FIG. 4. (Color online) (a) Magnetization curves of Co(d_{Co} =1.5 ML)/Cu(110)-(2×3)N at T=57, 74, and 85 K recorded by the longitudinal MOKE along [001]. (b) Temperature dependence of saturated Kerr rotation angles for d_{Co}=1.5, 2.0, and 3.0 ML.

2.0 ML Co is about three times smaller than that of 3.0 ML Co, although it would be 1.5 times smaller if the Co magnetic moment might not differ. This suggests the suppression of the Co magnetic moment at smaller coverages, as will be discussed below.

C. Analysis of XMCD

Before discussing the XMCD results, let us describe the XMCD analysis procedure first. Figure 5(a) shows the experimental geometry in the present XMCD measurements, where we will define the x-ray incidence angles θ_{in} and ϕ_{in};

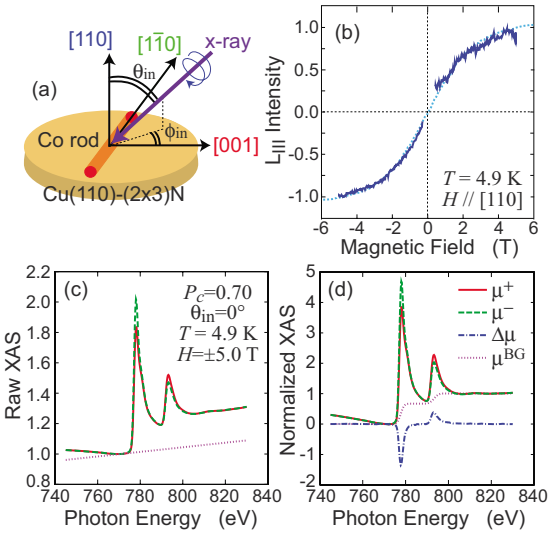

FIG. 5. (Color online) (a) Experimental geometry for the XMCD measurements of the present samples and [(b)–(d)] the examples of the XMCD analysis procedures. The data in (b)–(d) are given for Co(d_{Co}=0.8 ML)/Cu(110)-(2×3)N recorded at T =4.9 K and θ_{in}=0° (normal x-ray incidence). (b) shows the magnetization curve (blue solid line) obtained by recording the electron yield with the photon energy fixed at the L_3 peak top (~778 eV), together with a simulated curve (light blue dotted line). (c) gives circularly polarized XAS (red solid and green dashed lines) taken at H= ± 5 T and the estimated baseline (pink dotted line, see the text). (d) shows the normalized XAS μ^+ (red solid line) and μ^- (green dashed line), normalized XMCD spectra $\Delta\mu$ (dotted-dashed blue line), and the estimated background absorption μ^{BG} (pink dotted line).

θ_{in} is the polar angle with respect to the surface normal and ϕ_{in} is the azimuthal angle with respect to the [001] axis (perpendicular to the rod axis). Figure 5(b) gives a typical magnetization curve obtained by recording the electron yield with the photon energy fixed at the L_3 peak top (~778 eV). The magnetization curve provides valuable information on magnetic anisotropic constants and is also useful to estimate the saturated magnetization that is required in the XMCD data analysis. Details will be described below.

Figure 5(c) shows a pair of raw circularly polarized XAS. The electron yield data were scaled with a value at a certain photon energy (~770 eV) because of arbitrary units in the electron yield spectra, and the spectra in Fig. 5(c) are essentially raw data experimentally obtained. In Fig. 5(c), a linear baseline is also drawn, which is estimated so that the post-edge background absorption can be flat. Such a baseline subtraction minimizes the errors in the estimation of the white line intensity. In the present XAS and XMCD analysis, we might care for possible differences in the background electron yield between the N-terminated and clean Cu(110) surfaces due to the N K-edge absorption. The N absorption jump is however small enough (only a few percent with respect to the background yield) to discuss the Co L-edge spectra comparatively.

After the subtraction of the linear baseline from the raw spectra, the spectra are normalized with the $L_{3,2}$-edge jumps to yield a pair of the normalized circularly polarized XAS μ^+ and μ^-. In the case of thick films, the self-absorption correction is needed since the x-ray penetration depth is not sufficiently large compared to the electron escape depth.[22] The self-absorption correction can straightforwardly be performed when the film is assumed to be uniformly flat.[23] In the present samples, the spectra for the Co films thicker than 1 ML were corrected, although the corrections are not so huge except for d_{Co}=8.8 ML.

The XMCD spectra $\Delta\mu$ are obtained by evaluating $\Delta\mu = (\mu^+ - \mu^-)/(|P_c|f)$, where μ^+ and μ^- are the self-absorption corrected XAS, if the correction is performed. f is the additional normalization factor other than P_c. When the magnetization **M** is not parallel to the x-ray wave vector **k**, the scaling factor f=cos $\theta_{\mathbf{M},\mathbf{k}}$ should be included ($\theta_{\mathbf{M},\mathbf{k}}$ is the angle between **M** and **k**). On the other hand, the XMCD spectra $\Delta\mu$ in the saturated magnetization can be estimated by introducing the factor $f=M(H)/M_{sat}$ [$M(H)$ and M_{sat} are the measured and saturated magnetizations, respectively] as long as $M(H)$ is close to M_{sat}. The circularly polarized XAS in Figs. 5(c) and 5(d) were taken at H= ± 5 T, where the magnetization $M(H)$ is almost saturated as seen in Fig. 5(b). A small correction using $f=M(H)/M_{sat}$ is however more appropriate. $f=M(H)/M_{sat}$ can be estimated by the simulation of the magnetization curve using some simple phenomenological model [light blue dotted line in Fig. 5(b)]. Details of the simple model will be described below. The f value is found to be 0.908 in Fig. 5(b).

The XMCD sum-rule analysis is subsequently performed using the formulas of the orbital magnetic moment[24] and the spin magnetic moment.[25] First, the ratio between the orbital and effective spin magnetic moments, m_{orb}/m_{spin}^{eff}, is obtained by the formula as

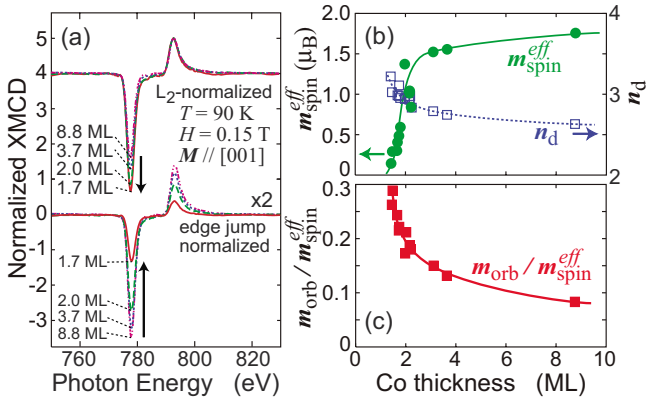

FIG. 6. (Color online) (a) Co L-edge XMCD spectra of Co/Cu(110)-(2×3)N at T=90 K and $H=\pm 0.15$ T, normalized with the $L_{3,2}$-edge jumps (lower, ×2 magnified) and the L_2 XMCD intensities (upper, +4 shifted). The x-ray incidence direction is $(\theta_{\rm in},\phi_{\rm in})=(60°,0°)$. (b) Co thickness dependence of the effective spin magnetic moment $m_{\rm spin}^{\rm eff}$ (left axis, green solid circles and green solid line) and the Co 3d hole number n_d (right axis, blue open squares and blue dotted line). (c) Co thickness dependence of the ratio between the orbital and effective spin magnetic moments, $m_{\rm orb}/m_{\rm spin}^{\rm eff}$.

$$\frac{m_{\rm orb}}{m_{\rm spin}^{\rm eff}}=\frac{\int_{L_3+L_2}\Delta\mu dE}{\int_{L_3}\Delta\mu dE-2\int_{L_2}\Delta\mu dE}. \quad (1)$$

Subsequently, the 3d hole number, n_d, is estimated as

$$n_d=C\int_{L_3+L_2}(\mu^{\rm av}-\mu^{\rm BG})dE, \quad (2)$$

where $\mu^{\rm av}=(\mu^+ +\mu^-)/2$ and $\mu^{\rm BG}$ is the background absorption as shown in Fig. 5(d). The proportional constant C is obtained by the standard spectrum of some reference material whose n_d is known. In the present analysis, the XMCD spectra of Co(3 ML)/Cu(001) and much thicker Co film (both n_d are assumed to be 2.50) were used as standards.[17,26] Consequently, the effective spin magnetic moments $m_{\rm spin}^{\rm eff}=m_{\rm spin}+7m_T$ ($m_{\rm spin}$ as the spin magnetic moment and m_T as the magnetic-dipole term) are evaluated as

$$\frac{m_{\rm spin}^{\rm eff}}{\mu_B}=-\frac{C}{3}\left(\int_{L_{\rm III}}\Delta\mu dE-2\int_{L_{\rm II}}\Delta\mu dE\right), \quad (3)$$

where μ_B is the Bohr magneton. Note that usually m_T cannot be neglected in magnetic ultrathin films. m_T can be estimated by measuring the angle dependence of the XMCD spectra under the saturated magnetization condition. This will be discussed in Sec. III E.

D. XMCD in $d_{\rm Co}>1.4$ ML

Figure 6(a) shows the thickness dependence of the Co L-edge XMCD spectra of Co/Cu(110)-(2×3)N at T=90 K, $H=\pm 0.15$ T, and $(\theta_{\rm in},\phi_{\rm in})=(60°,0°)$. The XMCD spectra were normalized with the $L_{3,2}$-edge jumps or the L_2 XMCD top intensities. The normalization factor f is given as $f=\cos\theta_{\mathbf{M},\mathbf{k}}=\cos 30°$ because the perpendicular component of the magnetization is found to be negligibly small under the present small magnetic field of $H=\pm 0.15$ T and the magnetization is aligned nearly along the easy axis of [001]. The lower series of the XMCD spectra clearly exhibits the enhancement of the XMCD signal with increasing the Co coverage. On the other hand, in the upper series, the L_3 negative peak intensity is enlarged with decreasing the Co coverage. This indicates the enhancement of the ratio of the orbital magnetic moment with respect to the spin magnetic moment.

The results of the sum-rule analysis are plotted in Figs. 6(b) and 6(c). The thermally averaged effective spin magnetic moment $m_{\rm spin}^{\rm eff}$ and the 3d hole number n_d are plotted in Fig. 6(b). $m_{\rm spin}^{\rm eff}$ is slightly reduced with decreasing $d_{\rm Co}$ from 8.8 to 2.0 ML and is abruptly suppressed from 2.0 to 1.4 ML. The abrupt reduction in $m_{\rm spin}^{\rm eff}$ should be caused mainly by the temperature effect and the critical thickness at T=90 K is thus estimated as $d_c\sim 1.4$ ML. The increase in n_d is again found with decreasing $d_{\rm Co}$. As discussed already in Fig. 2(c), this finding implies that the surface Co atom is cationic due to the formation of the Co-N bonds. The ratio of the orbital magnetic moment with respect to the effective spin magnetic moment, $m_{\rm orb}/m_{\rm spin}^{\rm eff}$, is plotted in Fig. 6(c). As expected in the upper spectral series in Fig. 6(a), the orbital magnetic moment is relatively enhanced with decrease in $d_{\rm Co}$. The values of $m_{\rm orb}/m_{\rm spin}^{\rm eff}$ are larger than 0.2 in $d_{\rm Co}<2$ ML, which is significantly greater than those of the Co films on Cu(001): 0.10 for 2 ML (Ref. 27) and 0.16 ± 0.02 for 0.4 ML.[17]

E. Magnetic properties of $d_{\rm Co}=0.8$ ML

In order to obtain information on magnetic anisotropy of the present nanorods, 0.8 ML Co on Cu(110)-(2×3)N that shows well separated nanorods was examined in the second run of the XMCD measurements. Angle-dependent XMCD spectra were recorded at T=4.9 K with a magnetic field up to H=5 T. Figure 7(a) shows the XMCD spectra taken at three different incidence angles of $\theta_{\rm in}$=0°, $(\theta_{\rm in},\phi_{\rm in})=(55°,90°)$ and $(55°,0°)$, which were normalized with the $L_{3,2}$-edge jumps or L_2 peak top intensity. The normalization factor of $f|P_c|$ is also included, where $f=M(H)/M_{\rm sat}$ is estimated from the magnetization curves in Fig. 7(b). The intensity of the L_3 peak is considerably different, implying significant angle dependence of the orbital magnetic moments.

The magnetization curves shown in Fig. 7(b) were recorded with the electron yield at the L_3 peak energy. The data in the vicinity of H=0 were omitted due to strong suppression of the electron yield by the Lorentz force. The magnetizations are found to be almost saturated at $H=\pm 5$ T for all the axes. The noticeably smoothed shape of the magnetization curves indicates a small size of the spin block (paramagneticlike behavior) in the present nanorods.

The magnetization curves in Fig. 7(b) were simulated using a simple second-order magnetic anisotropy model to deduce the macroscopic magnetic anisotropy constants. Assuming the two magnetic anisotropy constants K_θ and K_ϕ caused by the polar (film origin) and azimuthal (rod origin) anisotro-

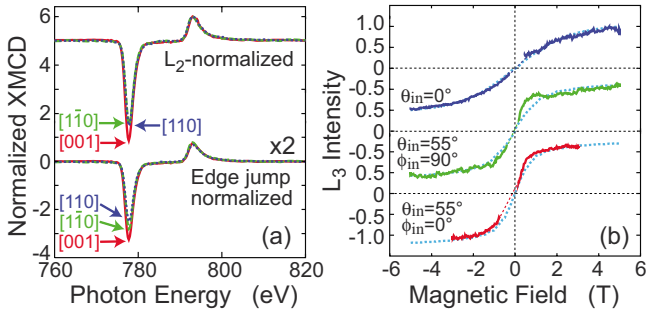

FIG. 7. (Color online) (a) Co L-edge XMCD spectra of Co/Cu(110)-(2×3)N (d_{Co}=0.8 ML) at T=4.9 K and $H=\pm 5.0$ T for $\theta_{in}=0°$ (blue dotted line, denoted as [110]) and $(\theta_{in},\phi_{in})=(55°,90°)$ (green dashed, [1$\bar{1}$0]) and $H=\pm 3.0$ T for $(\theta_{in},\phi_{in})=(55°,0°)$ (red solid, [001]). The lower and upper spectra correspond to those normalized with the edge jumps (×2 magnified) and the L_2 peak top intensity (+5 shifted), respectively. (b) Magnetization curves at T=4.9 K recorded with the L_3 peak top for the same incident angles as in (a). The simulated magnetization curves (light blue dotted lines) using a simple magnetic anisotropy model are also shown (see text for details).

pies, the magnetic anisotropy energy E_a is phenomenologically given as

$$E_a = K_\theta \cos^2\theta + K_\phi \sin^2\theta \sin^2\phi - \boldsymbol{\mu}\cdot\mathbf{H}, \tag{4}$$

where θ and ϕ are, respectively, the polar and azimuthal angles of the magnetic moment $\boldsymbol{\mu}$. The shape anisotropy is implicitly included in K_θ and K_ϕ. The fourth-order cubic magnetic anisotropy that determines the easy axis of the bulk cubic crystal is neglected because the film thickness is less than 1 ML in the present system.

Since the paramagneticlike magnetization curves were observed in Fig. 7(b), the finite-temperature effect due to a small size of the spin block should be considered. The classical Boltzmann distribution function $\rho=\exp[-NE_a/k_BT]$ was assumed in the simulation, where k_B is the Boltzmann constant and N is the number of atoms in one spin block. Due to the exchange interaction, the magnetic moment in each Co atom does not have an independent freedom but moves collectively within each spin block consisting of N atoms. The simulations were performed using the Monte Carlo method. The results of the simulated magnetization curves are also depicted in Fig. 7(b).

The parameters were determined as $K_\theta=(1.2\pm 0.1)\times 10^{-4}$ eV/atom, $K_\phi=(2.0\pm 0.5)\times 10^{-5}$ eV/atom, and $N=15\pm 5$ (atom). The size of the magnetization unit should be much smaller than the number of atoms in a nanorod but is exactly identical to the value of the Co atomic wire at 45 K.[1] The value of N however includes some ambiguity such as inhomogeneity of the nanorod length and will not be discussed in detail. The magnetic anisotropy constants obtained are nevertheless meaningful. This is because the spin block size N does not contribute to the slope of the magnetization curve but to the smooth shape, while the anisotropy constants exclusively determine the slope of the magnetization curve. The polar magnetic anisotropy K_θ that makes the surface normal the hardest axis is found to be much larger than that of the rod-axial anisotropy. The K_θ value is significantly larger than that of uniaxial anisotropy of bulk hcp Co (40 μeV/atom) (Ref. 28) but is rather smaller than the one in 0.4 ML Co on Cu(001) (1.8×10^{-4} eV/atom).[17]

TABLE I. Results of the sum-rule analysis of Co in Co(0.8 ML)/Cu(110)-(2×3)N. The 3d hole number n_d, the orbital magnetic moment m_{orb}, and the effective spin magnetic moment m_{spin}^{eff} are given for each experimental XMCD spectra. The estimated errors are shown in parentheses.

θ°	ϕ°	n_d	m_{orb} (μ_B)	m_{spin}^{eff} (μ_B)
55	0	3.11(15)	0.265(10)	1.15(6)
55	90	3.10(15)	0.192(10)	1.12(6)
0		3.10(15)	0.171(10)	1.04(6)

The XMCD spectra were similarly analyzed using the sum rules.[24,25] The obtained orbital and effective spin magnetic moments are summarized in Table I. As expected in Fig. 7(a), the orbital magnetic moment is the largest in the [001] spectrum. The effective spin magnetic moment m_{spin}^{eff} is found to depend on the x-ray incidence angle slightly, indicating the presence of a small magnetic-dipole term m_T. The 3d hole number n_d is considerably larger than the bulk Co one (n_d=2.50), again confirming that the Co atoms are cationic due to the formation of the Co-N bonds.

These experimental results further give the magnetic-dipole terms and the intrinsic spin magnetic moment[29,30] since the angle dependence of the saturated magnetization was measured owing to the usage of the superconducting magnet at low temperature. In the present twofold system, the relations of the angle dependence are

$$m_{orb}(\theta,\phi) = m_{orb}^x \sin^2\theta\cos^2\phi + m_{orb}^y \sin^2\theta\sin^2\phi + m_{orb}^z \cos^2\theta, \tag{5}$$

$$m_T(\theta,\phi) = m_T^x \sin^2\theta\cos^2\phi + m_T^y \sin^2\theta\sin^2\phi + m_T^z \cos^2\theta, \tag{6}$$

$$m_{spin}^{eff}(\theta,\phi) = m_{spin} + 7m_T(\theta,\phi), \tag{7}$$

where θ and ϕ are again, respectively, the polar and azimuthal angles of the magnetic moment and m_{orb}^α and m_T^α ($\alpha=x$, y, and z) are the α components of the orbital and magnetic-dipole moments, respectively. Note that the x ($\phi=0°$) and y ($\phi=90°$) axes correspond to the [001] (perpendicular to the rod) and [1$\bar{1}$0] (parallel to the rod axis) directions, respectively. For the magnetic-dipole terms, a general formula as

$$m_T^x + m_T^y + m_T^z = 0 \tag{8}$$

is also valid. When the XMCD data set of three independent incidence angles is available, all the quantities in Eqs. (5)–(7) can be evaluated because no angle dependence of the spin magnetic moment m_{spin} is expected.

TABLE II. Results of the angle-dependence analysis of Co in Co(0.8 ML)/Cu(110)-(2×3)N. The orbital magnetic moment m_{orb}, the magnetic-dipole moment m_T, and the spin magnetic moment m_{spin} are given. The estimated errors are shown in parentheses.

Axis	m_{orb} (μ_B)	m_T (μ_B)	m_{spin} (μ_B)
001	0.31(2)	0.010(5)	
$1\bar{1}0$	0.20(2)	0.004(5)	1.14(10)
110	0.17(2)	−0.014(5)	

The results for the component analysis are tabulated in Table II. The orbital magnetic moment increases in the sequence of [110], [$1\bar{1}0$], and [001], which is at least qualitatively consistent with the above magnetic anisotropy constants K_θ and K_ϕ; the [001] axis is the easy axis, while the [110] axis is the hardest one. This is also consistent with the thicker Co results shown in Sec. III D. It is concluded that the magnetic anisotropy in Co/Cu(110)-(2×3)N with d_{Co} =0.8 ML is dominated by the magnetocrystalline anisotropy as in the cases of somewhat coalescent Co nanorods (d_{Co} >1.5 ML) and also Co islands on clean Cu(110) and that the magnetic anisotropy originates from the anisotropic spin-orbit interaction.[31,32]

Note also that the spin magnetic moment obtained ($1.14\mu_B$) is significantly smaller than those of the Co thin films as well as bulk hcp Co: $1.55\mu_B$ for bulk Co, $1.77\mu_B$ for Co(2.1 ML)/Cu(001),[33] $1.79\mu_B$ for Co(0.4 ML)/Cu(001),[17] and $2.1\mu_B$ for Co atomic wire on Pt(997).[1,2] The small spin magnetic moment in Co may originate from the strong covalent bonds with the N atom in the present nanorods, this being partly exemplified from larger *d*-hole numbers as given above.

IV. CONCLUSIONS

In this work, structural and magnetic properties of self-assembled Co nanorods grown on Cu(110)-(2×3)N were investigated by LEED, AES, MOKE, and XMCD. The N atom is found to locate always at the surface even after 5 ML Co deposition. The N atom acts as a surfactant and the formation of the surface Co-N bonds makes the surface Co atoms cationic. The magnetic easy axis was found to be perpendicular to the rod axis within the substrate plane from the angle-dependent magnetization curves of d_{Co}=2.0 and 0.8 ML, recorded by the MOKE and XMCD measurements. The polar and azimuthal magnetic anisotropy constants of 0.8 ML Co estimated from the magnetization curves obtained by the XMCD measurements at T=4.9 K and up to H = ±5 T exhibit larger planar magnetic anisotropy than the rod-axial anisotropy. Significant enhancement of the orbital magnetic moment along the [001] direction was correspondingly detected by the angle-dependent XMCD measurements of 0.8 ML Co. This implies that the magnetic anisotropy of the Co nanorods is dominated by the magnetocrystalline anisotropy, irrespective of the Co thickness down to 0.8 ML, and is determined by the anisotropic spin-orbit interaction. Temperature and magnetic-field dependent magnetization curves from MOKE and XMCD were significantly smoothed due to the finite length of the present Co nanorods.

ACKNOWLEDGMENTS

The present authors gratefully acknowledge the staffs of UVSOR-II in IMS, especially E. Shigemasa and E. Nakamura for their sincere technical help in installing our XMCD apparatus. The authors are also grateful for the financial support of Grant-in-Aid for Scientific Research (Grants No. 15201029, No. 15087211, and No. 16710093) from Ministry of Education, Culture, Sports, Science and Technology (MEXT), Japan and also of Nanotechnology Network Project of MEXT.

*yokoyama@ims.ac.jp

[1] P. Gambardella, A. Dallmeyer, K. Maiti, M. C. Malagoli, W. Eberhardt, K. Kern, and C. Carbone, Nature (London) **416**, 301 (2002).
[2] P. Gambardella, A. Dallmeyer, K. Maiti, M. C. Malagoli, S. Rusponi, P. Ohresser, W. Eberhardt, C. Carbone, and K. Kern, Phys. Rev. Lett. **93**, 077203 (2004).
[3] H. J. Elmers, J. Hauschild, H. Höche, U. Gradmann, H. Bethge, D. Heuer, and U. Köhler, Phys. Rev. Lett. **73**, 898 (1994).
[4] H. J. Elmers, J. Hauschild, and U. Gradmann, Phys. Rev. B **54**, 15224 (1996).
[5] J. Shen, R. Skomski, M. Klaua, H. Jenniches, S. S. Manoharan, and J. Kirschner, Phys. Rev. B **56**, 2340 (1997).
[6] J. Hauschild, H. J. Elmers, and U. Gradmann, Phys. Rev. B **57**, R677 (1998).
[7] H. Fujisawa, S. Shiraki, M. Furukawa, M. Nantoh, M. Kawai, T. Nakamura, and T. Muro, J. Electron Spectrosc. Relat. Phenom. **144-147**, 519 (2005).
[8] O. Fruchart, M. Klaua, J. Barthel, and J. Kirschner, Phys. Rev. Lett. **83**, 2769 (1999).
[9] F. Komori, K. D. Lee, K. Nakatsuji, T. Iimori, and Y. Q. Cai, Phys. Rev. B **63**, 214420 (2001).
[10] S. M. York and F. M. Leibsle, Phys. Rev. B **64**, 033411 (2001).
[11] J. Fassbender, G. Güntherodt, C. Mathieu, B. Hillebrands, R. Jungblut, J. Kohlhepp, M. T. Johnson, D. J. Roberts, and G. A. Gehring, Phys. Rev. B **57**, 5870 (1998).
[12] W. L. Ling, Z. Q. Qiu, O. Takeuchi, D. F. Ogletree, and M. Salmeron, Phys. Rev. B **63**, 024408 (2000).
[13] E. Gu, S. Hope, M. Tselepi, and J. A. C. Bland, Phys. Rev. B **60**, 4092 (1999).
[14] S. Hope, E. Gu, M. Tselepi, M. E. Buckley, and J. A. C. Bland, Phys. Rev. B **57**, 7454 (1998).
[15] T. Nakagawa, H. Watanabe, and T. Yokoyama, Phys. Rev. B **71**, 235403 (2005).
[16] T. Gejo, Y. Takata, T. Hatsui, M. Nagasono, H. Oji, N. Kosugi, and E. Shigemasa, Chem. Phys. **289**, 15 (2003).

[17] T. Nakagawa, Y. Takagi, Y. Matsumoto, and T. Yokoyama, Jpn. J. Appl. Phys. **47**, 2132 (2008).
[18] X.-D. Ma, D. I. Bazhanov, O. Fruchart, T. Yokoyama, F. Yildiz, M. Przybylski, V. Stepanyuk, and J. Kirschner (unpublished).
[19] D. Sekiba, S. Doi, K. Nakatsuji, and F. Komori, Surf. Sci. **590**, 138 (2005).
[20] H. Wende, D. Arvanitis, M. Tischer, R. Chauvistré, H. Henneken, F. May, and K. Baberschke, Phys. Rev. B **54**, 5920 (1996).
[21] P. Poulopoulos, P. J. Jensen, A. Ney, J. Lindner, and K. Baberschke, Phys. Rev. B **65**, 064431 (2002).
[22] R. Nakajima, J. Stöhr, and Y. U. Idzerda, Phys. Rev. B **59**, 6421 (1999).
[23] X. D. Ma, T. Nakagawa, and T. Yokoyama, Surf. Sci. **600**, 4605 (2006).
[24] B. T. Thole, P. Carra, F. Sette, and G. van der Laan, Phys. Rev. Lett. **68**, 1943 (1992).
[25] P. Carra, B. T. Thole, M. Altarelli, and X. Wang, Phys. Rev. Lett. **70**, 694 (1993).
[26] O. Hjortstam, J. Trygg, J. M. Wills, B. Johansson, and O. Eriksson, Phys. Rev. B **53**, 9204 (1996).
[27] M. Tischer, O. Hjortstam, D. Arvanitis, J. H. Dunn, F. May, K. Baberschke, J. Trygg, J. M. Wills, B. Johansson, and O. Eriksson, Phys. Rev. Lett. **75**, 1602 (1995).
[28] G. Bate, J. Magn. Magn. Mater. **100**, 413 (1991).
[29] J. Stöhr and H. König, Phys. Rev. Lett. **75**, 3748 (1995).
[30] N. Nakajima, T. Koide, T. Shidara, H. Miyauchi, H. Fukutani, A. Fujimori, K. Iio, T. Katayama, M. Nývlt, and Y. Suzuki, Phys. Rev. Lett. **81**, 5229 (1998).
[31] P. Bruno, Phys. Rev. B **39**, R865 (1989).
[32] G. van der Laan, J. Phys.: Condens. Matter **10**, 3239 (1998).
[33] P. Srivastava, F. Wilhelm, A. Ney, M. Farle, H. Wende, N. Haack, G. Ceballos, and K. Baberschke, Phys. Rev. B **58**, 5701 (1998).